Implementation of Real-Time Digital Twin of Dual Active Bridge Converter in Electrolyzer Applications

Deshmukh, Rohan Shailesh ; Rituraj, Gautam; Lock, Niels; Vahedi, Hani; Shekhar, Aditya; Bauer, Pavol

DOI
10.1109/IECON51785.2023.10312274

Publication date
2023

Document Version
Final published version

Published in
Proceedings of the IECON 2023- 49th Annual Conference of the IEEE Industrial Electronics Society

Implementation of Real-Time Digital Twin of Dual Active Bridge Converter in Electrolyzer Applications

Rohan Shailesh Deshmukh (*Student Member, IEEE*) , Gautam Rituraj (*Member, IEEE*), Niels Lock, Hani Vahedi (*Senior Member, IEEE*), Aditya Shekhar (*Member, IEEE*), Pavol Bauer (*Senior Member, IEEE*)
Electrical Sustainable Energy Department, Delft University of Technology, The Netherlands
r.s.deshmukh@tudelft.nl

IECON 2023- 49th Annual Conference of the IEEE Industrial Electronics Society | 979-8-3503-3182-0/23/$31.00 ©2023 IEEE | DOI: 10.1109/IECON51785.2023.10312274

***Abstract*—Power electronics converters (PEC) play a crucial role in interfacing renewable energy systems and electrolyzers to ensure a high production yield of green hydrogen. The design of such PEC is not straightforward due to the safety hazards of using multiple electrolyzer stacks and converter modules at industrial levels. Therefore, real-time simulations should be conducted to ensure the converter design satisfies all the requirements before deploying it on-site. This paper presents a real-time digital twin (RTDT) of a 10 kW dual-active bridge converter interfaced with an electrolyzer. OPAL-RT simulator (eHS toolbox) is used for RTDT. Finally, the voltage across the series inductance and current flowing through it are presented for the open-loop operation of DAB.**

***Index Terms*—Dual Active Bridge, Electrolyzer, and Real-Time Digital Twin.**

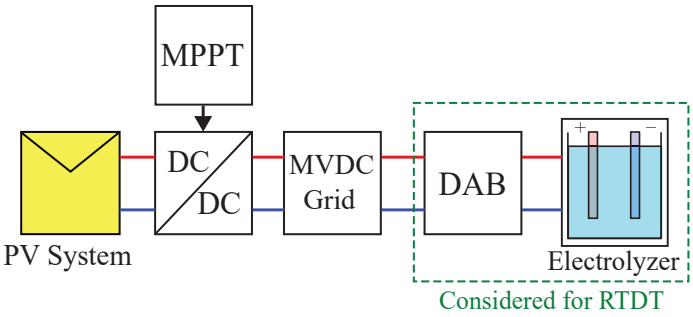

Fig. 1: PV integrated electrolyzer system. The highlighted area is used for developing RTDT.

I. Introduction

Over the years, the concept of Digital Twin (DT) has been emphasized by both industry and academia [1]. DT can be defined in multiple ways; therefore, it varies depending on the application. From the perspective of developing power electronics converters (PEC), a DT can be defined as a virtual representation of a physical power electronics converter, including its characteristics, behavior, and performance. DTs are commonly utilized for system monitoring, diagnostics, prognostics, and health monitoring (PHM), as well as for hardware-in-the-loop (HIL) simulations to validate controllers and to conduct scenario and risk assessments [2].

Various literature showcases the potential of a DT in aerospace [3], power systems [4], [5], electric vehicles (EVs) [6], and the electrolyzer [7], [8]. In [3], the DT of the space vehicle for the NASA Apollo mission is developed with a focus on simulating the space conditions to facilitate astronaut training. A methodology is proposed in [4] to implement digital twins for online analysis of power systems. The use of DT for estate evaluation of a power transformer has been studied in [5]. In [6], the monitoring and prediction of an EV's health are carried out using a DT, and the results are validated with a MATLAB/Simulink model. In [7], a DT of 500kW alkaline water electrolysis using Python and gPROMS is presented for green hydrogen production. Thus, from the literature, it has been found that RTDT for interfacing PEC in electrolyzer applications is yet to be explored.

Renewable energy resources play an important role in clean energy transition [9]–[11]. Electrolysis exhibits tremendous potential to generate green hydrogen with the help of renewable electricity. However, when scaled up to an industrial level, the design of such converters is more complex. Obligatory design requirements include the presence of galvanic isolation between the input stage and the output stage per ISO22734:2020 and ISO:19880-1:2020 standards. Electrolysis requires low voltage and extremely high current for its' optimal operation [12]. Therefore, before physically installing the converter within the system, it must be evaluated under different test conditions and contingencies. Besides that, based on the literature study in [12], the Dual Active Bridge (DAB) converter was identified as a suitable candidate to interface with the electrolyzer. It offers the ability to have a series-parallel arrangement [13], which can be beneficial when developing a modular system architecture for high-power electrolysis.

Fig. 1 shows the Photovoltaic (PV)-integrated electrolyzer system. The integration of the PV system into the medium voltage direct-current (MVDC) grid can be achieved by utilizing a DC-DC converter based on Maximum Power Point Tracking (MPPT). Furthermore, the DAB DC-DC converter is a power electronics interface (PEI) connecting the MVDC grid to the electrolyzer. This paper focuses on implementing an RTDT of a DAB converter integrated with an electrolyzer, as highlighted in Fig. 1. This RTDT would be a building block

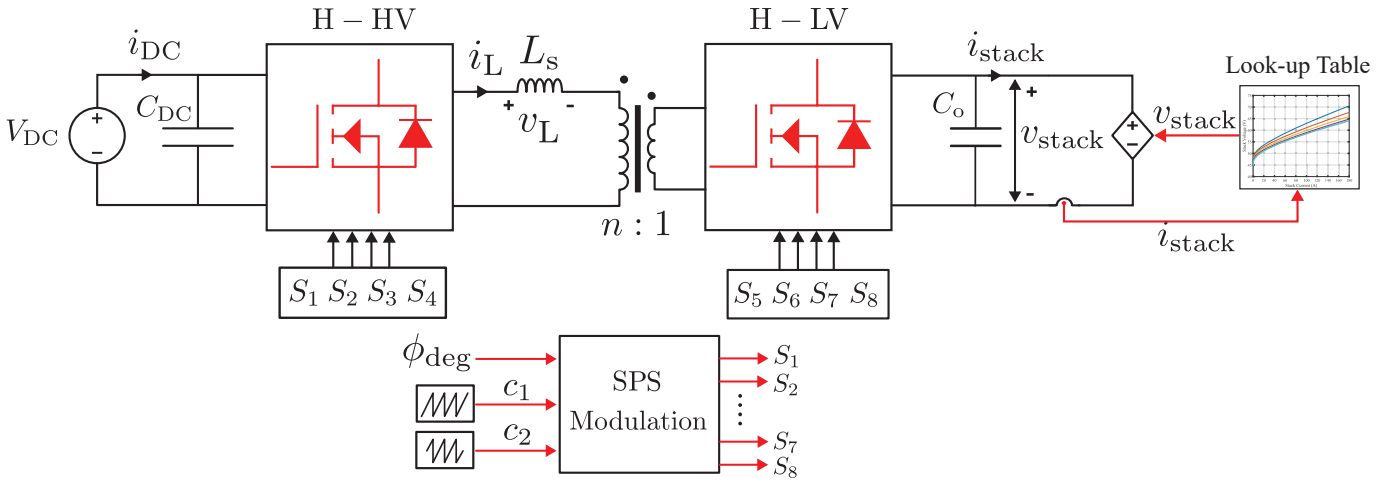

Fig. 2: Illustration for the real-time implementation of the highlighted part in Fig. 1.

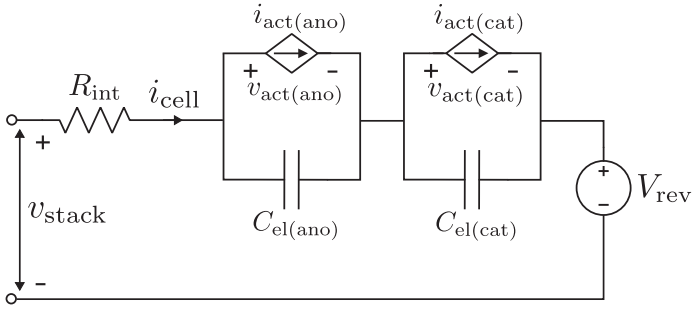

Fig. 3: Electrical Representation of an Alkaline electrolyzer.

for developing an RTDT of modular DAB configurations. The rest of the paper is organized as follows: Section II presents the system description, including modeling the alkaline electrolyzer and DAB. It further explains the real-time simulator adopted in this work. Section III describes the model and I/O implementations in the OPAL-RT simulator. Results are presented and discussed in Section IV. Finally, the conclusions and future work are given in Section V.

II. System Description

Fig. 2 shows the schematic for the real-time implementation of the DAB-integrated electrolyzer (as highlighted in Fig. 1). The system has two main components: the DAB converter and the alkaline electrolyzer. The modeling approaches for both of these components have been explained briefly in this section. Besides that, the real-time simulator used in this work is also introduced.

A. Alkaline Electrolyzer Modeling

Being the most mature and commercially available technology, an alkaline electrolyzer has been chosen as the electrical load for the DAB converter. Fig. 3 shows the detailed electrical representation of an alkaline electrolyzer. Several modeling approaches have been reported in the literature [14]–[18]. However, the modeling approach used in [14] is adopted in this paper. From Fig. 3, the stack voltage v_{stack} can be expressed as

$$v_{stack} = N_s \cdot (V_{rev} + v_{act(ano)} + v_{act(cat)} + v_{int}) \quad (1)$$

where V_{rev} is the reversible cell voltage, N_s is the number of series connected cells, v_{int} is the ohmic potential, $v_{act(ano)}$ is the anode activation potential, and $v_{act(cat)}$ is the cathode activation potential. The expressions for V_{rev}, v_{int}, $v_{act(ano)}$, and $v_{act(cat)}$ are given in (2)-(5), respectively.

$$V_{rev} = V^0_{rev,T_k} + \frac{RT_k}{zF} \ln\left(\frac{(P - P_{KOH})^{1.5}}{a_{H_2O,KOH}}\right) \quad (2)$$

$$v_{act(ano)} = s \ln\left(\frac{i_{act(ano)}}{t} + 1\right) \quad (3)$$

$$v_{act(cat)} = v \ln\left(\frac{i_{act(cat)}}{w} + 1\right) \quad (4)$$

$$v_{int} = i_{cell} \cdot R_{int} = i_{cell} \frac{r}{A_{elect}}$$

where V^0_{rev,T_k} is the temperature dependent reversible voltage. R is the universal gas constant (JK^{-1}mol^{-1}). T_k is the cell temperature (K). P is the absolute pressure (bar), z is the number of electron moles transferred for 1 mol of the product, F is the Faraday constant (C mol^{-1}), P_{KOH} is the KOH vapor pressure (bar), and $a_{H_2O,KOH}$ is the water activity of the KOH solution. Besides that, the temperature-dependent constants are denoted as s, t, v, and w. Activation currents for the anode and cathode are represented as $i_{act(ano)}$ and $i_{act(cat)}$, respectively. r is the area-specific resistance of one of the electrolysis cells (Ωm^2). i_{cell} is the cell current. Finally, A_{elect} and R_{int} are the surface area of the electrode (m^2) and the internal resistance of the electrolyzer cell (Ω), respectively.

To integrate the electrolyzer with the DAB converter, it has been modeled as a current-controlled voltage source, as shown in Fig. 2. A lookup table is generated based on the

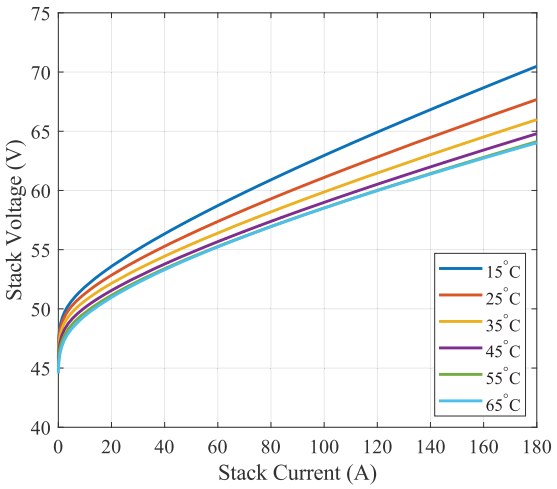

Fig. 4: Electrical characteristics of a 10 kW alkaline electrolyzer.

electrical characteristics shown in Fig. 4 (obtained using (2)), and therefore, the lookup table sets the stack voltage by measuring the stack current.

B. Dual Active Bridge Converter Modeling

The block diagram of the DAB isolated dc-dc converter is shown in Fig. 2. It consists of two H-bridges, H-HV and H-LV, representing the high-voltage side bridge and the low-voltage side bridge, respectively. Depending on the application, each bridge is isolated using a high-frequency (HF) transformer with a unity turn ratio or a step-up/step-down function.

The single-phase shift (SPS) modulation strategy, which is a classic modulation technique for DAB converters, has been chosen for this study. In this method, the duty cycle or the pulse width of the switching signals sent to both bridges is maintained fixed. However, the switching signals sent to one of the bridges are phase shifted by an angle ϕ.

The expression for the output power (P_{op}) of the DAB with single phase shift modulation can be expressed as

$$P_{\text{op}} = \frac{(D \cdot (1 - D)) \cdot V_{\text{DC}} \cdot V_{\text{o}} \cdot n}{2 \cdot f_{\text{sw}} \cdot L_{\text{s}}} \tag{5}$$

where V_{DC} is the input DC voltage, V_{o} is the output DC voltage, n is the turn ratio, L_s is the series inductance, and f_{sw} is switching frequency. Moreover, D is the phase shift duty cycle that can be expressed in terms of ϕ

$$D = \pi \cdot \phi \tag{6}$$

$$D = \left| \frac{1}{2} \cdot (1 - \Delta) \right| \tag{7}$$

$$\Delta = \sqrt{1 - \left(\frac{8 \cdot P_{\text{op}} \cdot L_{\text{s}} \cdot f_{\text{sw}}}{V_{\text{DC}} \cdot V_{\text{o}} \cdot n} \right)} \tag{8}$$

C. Real Time Simulator

The OP4610XG is a real-time simulator developed by OPAL-RT Technologies. Fig. 5 shows the OP4610XG simulator. It is a comprehensive simulation system that utilizes a Kintex 7 fully programmable gate array (FPGA). It includes a robust target computer, a flexible, high-speed front-end Processor, and a signal conditioning stage. The system is user-friendly with standard connectors such as DB37, DB9, or Fiber POF. Additionally, it provides six optional input/output LVDS links that can function in RS422 or Optical fiber mode, with RS422 being the default configuration. The lower part of the chassis houses the target computer, which can operate independently as a standalone computer in its' standard setup.

Fig. 5: OP4610XG Real-Time Simulator

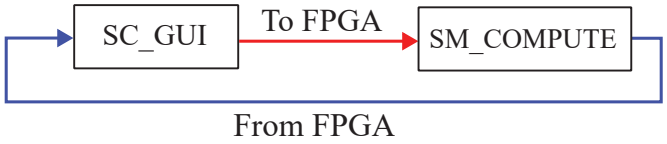

Fig. 6: Simulink model layout for execution within the real-time simulator.

III. Model and I/O Implementations

A MATLAB Simulink model cannot be directly used for real-time simulation in OPAL-RT. A typical representation of a Simulink model developed for being executed within the real-time simulator is shown in Fig. 6. Here, the Simulink model is divided into two subsystems: the graphical user interface (GUI), represented by the subsystem prefix "SC_" and the computation subsystem, represented by the subsystem prefix "SM_". Furthermore, the SC_GUI subsystem contains all the monitoring blocks, such as scopes, displays, etc., and the input parameters, such as constant blocks, sliders, etc. On the other hand, the SM_COMPUTE subsystem contains functions and, most importantly, the plant model that needs to run on the FPGA/CPU of the real-time simulator. Further explanation on these subsystems, including I/O, can be found below.

A. Graphical User Interface Subsystem

Since the model is implemented within the FPGA in this case, this subsystem contains three inputs: f_{sw}, D, and ϕ. These parameters are then sent to the computation subsystem. This has been illustrated in Fig. 7.

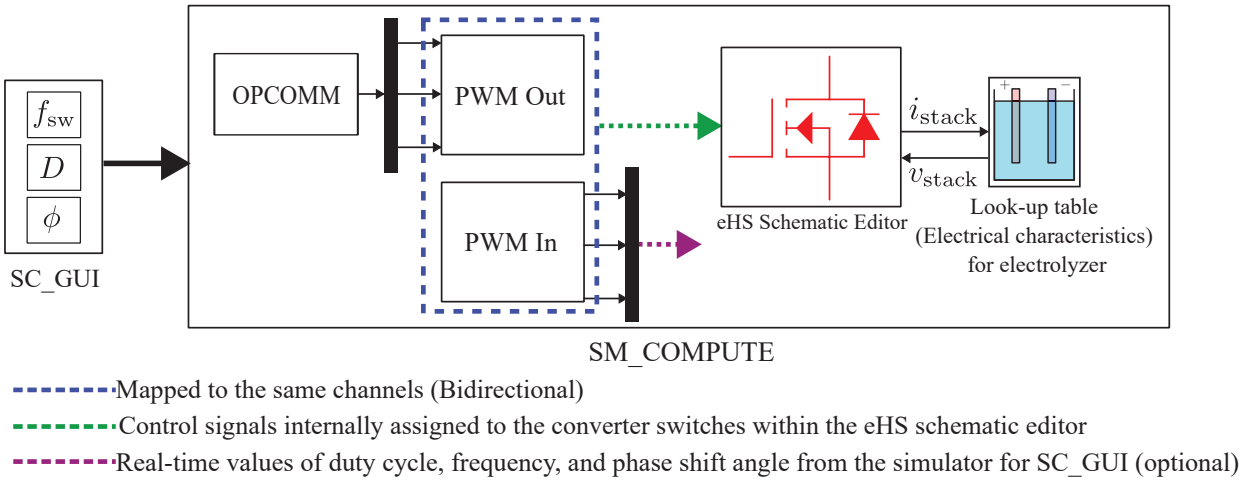

Fig. 7: Detailed layout of the subsystems implemented for the DAB RTDT.

B. Computation Subsystem

In the computation subsystem, the three outputs from the SC_GUI subsystem are provided to a PWM Out block via the OPCOMM block, as shown in Fig. 7. The OPCOMM block is necessary for simulating real-time communication links [19].

The CPU of an OPAL-RT simulator can perform computations with a time step as small as 5 μs. However, PEC typically operate at higher switching frequencies in tens of kilohertz to hundreds. In this case, executing computations within the CPU is not preferable due to the significant time step, which can result in information loss. Therefore, using FPGA becomes necessary as it can achieve a time step in the order of tens of nanoseconds.

To implement PEC topology within the FPGA, the eHS toolbox is utilized. It contains an electrical solver for the FPGA and a schematic editor for implementing the converter topology. The eHS block can accept inputs from Simulink or the FPGA. On the other hand, it can provide outputs to the Simulink scopes located within the SC_GUI subsystem and these signals at the FPGA output channels.

C. Bidirectional Digital I/O

The bidirectional digital card consists of sixteen channels. For the RTDT, channels 0 - 3 have been configured to behave as both a PWM output as well as a PWM input channel due to the bidirectional functionality of the card. Each pair corresponds to the complementary switches, i.e., channel 0 is complementary to channel 1, and channel 2 is complementary to channel 3. The four channels have been configured so that parameters such as f_{sw}, D, and ϕ can be changed on the go. However, with reference to the SPS modulation scheme, only the phase shift angle of channels 2 and 3 must be varied with respect to channels 0 and 1 at the fixed duty cycle of 50 %.

D. Analog Outputs

Four analog outputs are monitored in this RTDT: stack voltage, stack current, the voltage across the series inductance, and the primary transformer current. Channels 0 - 3 of the analog output card are configured within the eHS schematic editor with appropriate gains to avoid saturation.

IV. Results

This section presents the results of DAB operation with an electrolyzer under different power levels, as shown in Fig. 8. Here, the DAB parameters for a rated P_{op} of 10 kW at the rated V_o of 70 V, f_{sw} is set to be 20 kHz, n is 20, L_s is 100 μH, and V_{DC} is set to be 1400 V.

Fig. 8(a) shows the variation in stack power for five test cases of P_{op} (i.e., 10, 8, 1, 2.5, and 9 kW). These power levels are achieved at different ϕ, calculated using (6). At these power levels, the stack voltage, stack current, voltage across the series inductance, and the current flowing through it are shown in Fig. 8(b)-(f), respectively. Here, it can be observed that the peak value of the inductor current is almost similar for all power variations. However, a change in the slope of the inductor current is seen in Fig. 8(c)-(f) compared to the operation at rated P_{op}, as shown in Fig. 8(b), due to change in stack voltage for the same turns ratio. Moreover, a change in the stack current ripple is also seen at different power levels in Fig. 8(b)-(f).

V. Conclusions and Future Work

This paper implemented a real-time digital twin (RTDT) of a 10 kW DAB converter integrated with an alkaline electrolyzer. It comprehensively described the PV-integrated electrolyzer system and discussed the modeling of the alkaline electrolyzer and DAB converter. The implementation of these models within the real-time simulator environment has been explained in detail, along with the I/O configuration of the FPGA. Furthermore, the results for five test cases of operating power in an open-loop configuration, including stack voltage and current, the voltage across the series inductance, and the current flowing through it, are presented.

This study will be extended further to a closed-loop control configuration in future work. Besides that, the impact of

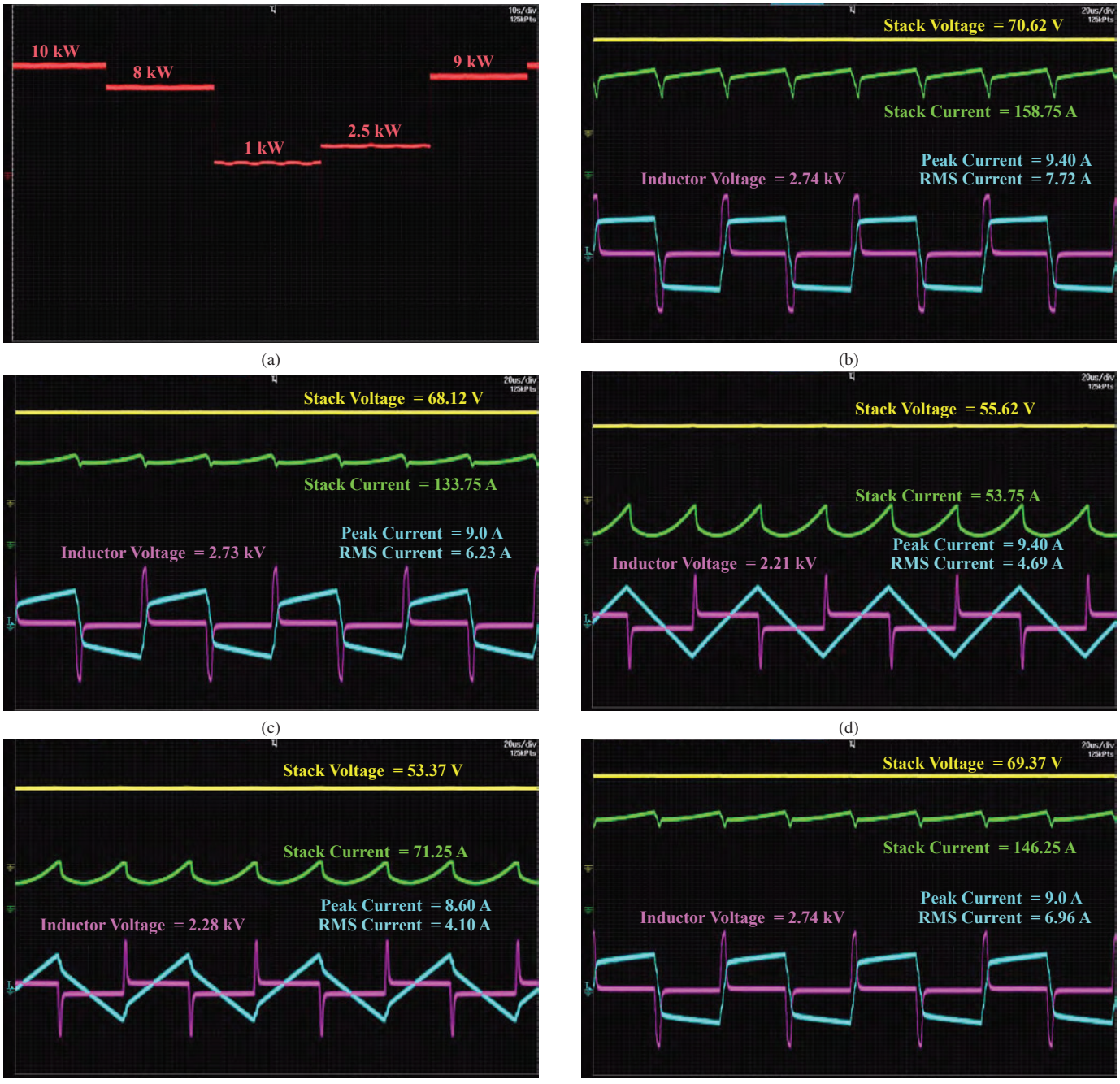

Fig. 8: (a) Stack power at different power levels and waveforms of stack voltage, stack current, inductor voltage and current at the mentioned power in Fig. 8(a), i.e., (b) 10 kW, (c) 8 kW, (d) 1 kW, (e) 2.5 kW, and (f) 9 kW.

different electrolyzer system architectures on the converter's performance will be evaluated.

REFERENCES

[1] F. Tao, H. Zhang, A. Liu, and A. Y. Nee, "Digital twin in industry: State-of-the-art," *IEEE Transactions on industrial informatics*, vol. 15, no. 4, pp. 2405–2415, 2018.

[2] A. Rasheed, O. San, and T. Kvamsdal, "Digital twin: Values, challenges and enablers from a modeling perspective," *Ieee Access*, vol. 8, pp. 21 980–22 012, 2020.

[3] E. Glaessgen and D. Stargel, "The digital twin paradigm for future nasa and us air force vehicles," in *53rd AIAA/ASME/ASCE/AHS/ASC structures, structural dynamics and materials conference 20th AIAA/ASME/AHS adaptive structures conference 14th AIAA*, 2012, p. 1818.

[4] M. Zhou and J. Yan, "A new solution architecture for online power system analysis," *CSEE Journal of Power and Energy Systems*, vol. 4, no. 2, pp. 250–256, 2018.

[5] P. Moutis and O. Alizadeh-Mousavi, "Digital twin of distribution power transformer for real-time monitoring of medium voltage from low voltage measurements," *IEEE Transactions on Power Delivery*, vol. 36,

no. 4, pp. 1952–1963, 2020.
[6] S. Venkatesan, K. Manickavasagam, N. Tengenkai, and N. Vijayalakshmi, "Health monitoring and prognosis of electric vehicle motor using intelligent-digital twin," *IET Electric Power Applications*, vol. 13, no. 9, pp. 1328–1335, 2019.
[7] Y. Shin, J. Oh, D. Jang, and D. Shin, "Digital twin of alkaline water electrolysis systems for green hydrogen production," in *Computer Aided Chemical Engineering*. Elsevier, 2022, vol. 49, pp. 1483–1488.
[8] A. Shekhar, G. Rituraj, R. Van Der Sande, M. Ahmadi, R. Deshmukh, P. Bauer, V. Nougain, A. Lekić, and P. Palensky, "Development of reliable power electronic systems using real time digital twin based power hardware-in-the-loop testbed," in *2023 IEEE Belgrade PowerTech*, 2023, pp. 1–6.
[9] H. Vahedi, M. Sharifzadeh, and K. Al-Haddad, "Modified seven-level pack u-cell inverter for photovoltaic applications," *IEEE Journal of Emerging and Selected Topics in Power Electronics*, vol. 6, no. 3, pp. 1508–1516, 2018.
[10] H. Vahedi, M. Sharifzadeh, K. Al-Haddad, and B. M. Wilamowski, "Single-dc-source 7-level chb inverter with multicarrier level-shifted pwm," in *IECON 2015 - 41st Annual Conference of the IEEE Industrial Electronics Society*, 2015, pp. 004 328–004 333.
[11] G. Rituraj, G. R. C. Mouli, and P. Bauer, "A comprehensive review on off-grid and hybrid charging systems for electric vehicles," *IEEE Open Journal of the Industrial Electronics Society*, vol. 3, pp. 203–222, 2022.
[12] R. S. Deshmukh, A. Shekhar, and P. Bauer, "Adaptive modularity for power electronics based electrolysis systems for green hydrogen," in *2022 IEEE 20th International Power Electronics and Motion Control Conference (PEMC)*, 2022, pp. 508–515.
[13] H. Akagi, S.-i. Kinouchi, and Y. Miyazaki, "Bidirectional isolated dual-active-bridge (dab) dc-dc converters using 1.2-kv 400-a sic-mosfet dual modules," *CPSS Transactions on Power Electronics and Applications*, vol. 1, no. 1, pp. 33–40, 2016.
[14] Ø. Ulleberg, "Modeling of advanced alkaline electrolyzers: a system simulation approach," *International journal of hydrogen energy*, vol. 28, no. 1, pp. 21–33, 2003.
[15] D. Falcão and A. Pinto, "A review on pem electrolyzer modelling: Guidelines for beginners," *Journal of Cleaner Production*, vol. 261, p. 121184, 2020.
[16] A. Ursúa, P. Sanchis, and L. Marroyo, *Chapter 14 - Electric Conditioning and Efficiency of Hydrogen Production Systems and Their Integration with Renewable Energies*, L. M. Gandía, G. Arzamendi, and P. M. Diguez, Eds. Elsevier, 2013.
[17] A. Ursúa and P. Sanchis, "Static-dynamic modelling of the electrical behaviour of a commercial advanced alkaline water electrolyser," *International journal of hydrogen energy*, vol. 37, no. 24, pp. 18 598–18 614, 2012.
[18] N. Gallandat, K. Romanowicz, and A. Züttel, "An analytical model for the electrolyser performance derived from materials parameters," *Journal of Power and Energy Engineering*, vol. 5, no. 10, pp. 34–49, 2017.
[19] "Opcomm," https://opal-rt.atlassian.net/wiki/spaces/PRD/pages/144180849/OpComm, accessed: 2023-06-15.